Dissecting out the effect of Ru-OAr bonding in a five-coordinate complex of ruthenium (II)[1]

Sebastien Monfette, João A. Duarte Silva, Serge I. Gorelsky, Scott J. Dalgarno, Eduardo N. dos Santos, Maria H. Araujo, and Deryn E. Fogg

Abstract: Blue Ru(*o*-cat)(PPh_3)$_3$ (**5**; *o*-cat = *ortho*-catecholate), obtained in 94% yield by reaction of $RuCl_2(PPh_3)_3$ (**4**) with dithallium catecholate, was characterized by NMR, MALDI-MS, IR, and single crystal X-ray analysis, and by a combined electronic spectroscopy and time-dependent density functional theory (TD-DFT) study. The frontier orbitals in **5** participate in a low-energy charge transfer excitation involving donation from the Ru-catecholate π bond (largely localized on catecholate) to a low-lying σ* orbital on Ru-$PPh_{3(apical)}$. The energy of this transition increases on binding a pyridine ligand in the sixth site.

Key words: ruthenium aryloxide, catecholate, phosphine, electronic spectroscopy, time-dependent DFT.

Résumé : Le Ru(*o*-cat)(PPh_3) bleu (**5**; *o*-cat = *ortho*-catécholate) qui est obtenu avec un rendement de 94% par réaction du $RuCl_2(PPh_3)_3$ (**4**) avec le catécholate de dithallium a été caractérisé par RMN, spectrométrie de masse "MALDI", spectroscopie IR et par diffraction des rayons X par un cristal unique ainsi que par une combinaison de spectroscopie électronique et d'une étude de théorie de la fonctionnelle de densité en fonction du temps. Les orbitales frontières du produit **5** participent dans une excitation par transfert de charge de basse énergie impliquant le don d'électron à partir de la liaison π du catécholate de ruthénium (principalement localisée sur le catécholate) vers une orbitale σ* de basse énergie du Ru-$PPh_{3(apical)}$. L'énergie de cette transition augmente lors de la fixation d'un ligand pyridine sur le sixième site.

Mots-clés : aryloxyde de ruthénium, catécholate, phosphine, spectroscopie électronique, théorie de la fonctionnelle de densité en fonction du temps.

[Traduit par la Rédaction]

Introduction

Olefin metathesis is now one of the most powerful methods in use for the construction of C=C bonds (1). Of the many well-defined catalysts developed for this versatile reaction, the Grubbs-class catalysts, $RuCl_2LL'$(=CHPh), have had the greatest impact in organic synthesis owing to their relative robustness and ease of handling. We have been engaged in a program of study focusing on the largely neglected (2) potential of the anionic sites to expand the modularity, tunability, and lifetime of the Ru-NHC catalysts (3) (NHC = *N*-heterocyclic carbene). Particular success has emerged for derivatives containing monodentate or κ^2-chelating aryloxide ligands (Fig. 1). These exhibit, inter alia, increased lifetime (for **1**), enhanced efficiency (**2** and **3**), and a high kinetic selectivity for cyclic vs. oligomeric products in macrocycle RCM (**2**, **3**; RCM = ring-closing metathesis) (3).

Emerging findings from our laboratory have focused our attention on the importance of the Ru-aryloxide electronic interactions in determining not merely catalyst activity, but also the kinetic bias toward RCM products. In the present work, we wished to evaluate the electronic interactions specific to the basal Ru-aryloxide moiety within the square pyramidal coordination geometry, unperturbed by the variety of additional bonding interactions present in the alkylidene complexes of Fig. 1. While five-coordinate Ru complexes containing monodentate phosphine and phenoxide ligands (e.g., $RuX(OPh)(PPh_3)_3$) would be suitable candidates for study, such species are unstable with respect to isomerization to piano-stool structures (Scheme 1) (4), unless the aryloxide ligand is stabilized by electron-withdrawing substituents that add to the complexity of our intended electronic analysis.

In earlier work, we established that σ–π isomerization of aryloxide donors in these labile, coordinatively unsaturated

Received 3 June 2008. Accepted 31 July 2008. Published on the NRC Research Press Web site at canjchem.nrc.ca on 25 November 2008.

This paper is dedicated to Professor Dick Puddephatt, in honour of his many contributions to chemistry and the Canadian chemistry community.

S. Monfette, S.I. Gorelsky, and D.E. Fogg.[2] Department of Chemistry, Center for Catalysis Research & Innovation, University of Ottawa, Ottawa ON K1N 6N5, Canada.
S.J. Dalgarno.[3] School of EPS-Chemistry, Heriot-Watt University, Edinburgh EH14 4AS Scotland.
J.A. Duarte Silva, E.N. dos Santos, and M.H. Araujo. Departamento de Química– ICEx, Universidade Federal de Minas Gerais, 31270–901 Belo Horizonte, Brazil.

[1]This article is part of a Special Issue dedicated to Professor R. Puddephatt.

[2]Corresponding author (e-mail: dfogg@uottawa.ca).

[3]Present address: Department of Chemistry, University of Missouri, 601 S. College Ave, Columbia, MO 65211, USA.

 doi:10.1139/V08-147

Fig. 1. Key Ru-aryloxide catalysts (3); one isomer shown for **2**. IMes = *N,N′*-bis(mesityl)imidazol-2-ylidene, py = pyridine.

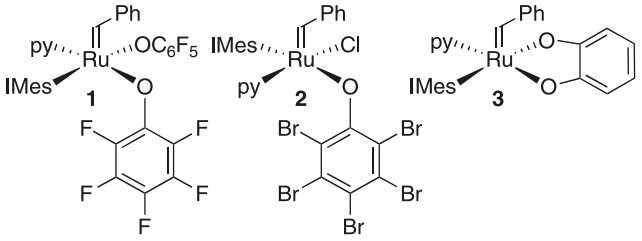

Scheme 1.

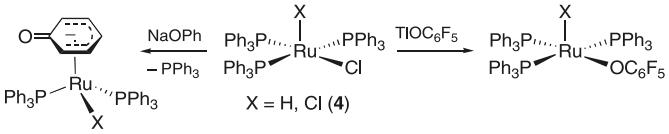

species is not inhibited by chelation within large (seven-membered) chelate rings (4*a*). The stability of the catecholate ligand in **3**, however, suggested that a smaller chelate might stabilize our target systems. We therefore sought to examine an alternative model complex, Ru(*o*-cat)(PPh_3)$_3$ (**5**, *o*-cat = *ortho*-catecholate). Here we describe the synthesis and structural characterization of **5** and an analysis of its frontier orbital interactions by electronic spectroscopy and time-dependent density functional theory (TD-DFT) calculations.

Results and discussion

Synthesis of Ru(*o*-cat)(PPh_3)$_3$ (5)

The addition of solid thallium catecholate to a homogeneous solution of $RuCl_2(PPh_3)_3$ **4** in THF caused a colour change from brown to deep blue within 1 h at room temperature, accompanied by precipitation of TlCl. ^{31}P NMR analysis of the crude reaction mixture indicated clean formation of a single Ru product, without liberation of PPh_3. The suspension was filtered through Celite, and the Ru product was isolated in 94% yield by precipitation from THF–hexanes. It was identified as Ru(κ^2-$O_2C_6H_4$)(PPh_3)$_3$ **5** (Scheme 2) on the basis of spectroscopic, crystallographic, and combustion analysis. This complex exhibits high air-sensitivity even in the solid state (possibly a function of the high-lying HOMO in this system; vide infra).

The anaerobic MALDI-TOF mass spectrum (5) of **5** revealed a well-defined isotope pattern for $[M–PPh_3]^{+\cdot}$ at *m*/*z* 734.4 Da. The facile elimination of one triphenylphosphine group in the gas phase probably reflects the steric pressure within the three approximately facial PPh_3 ligands. Retention of all three of these ligands in the solid state is confirmed by X-ray analysis, as discussed below; their retention in solution can be inferred from the ^{1}H NMR integration values as well as the absence of a signal for free PPh_3 in the ^{31}P NMR spectrum of the crude reaction mixture. Unexpectedly, however, a sharp ^{31}P{^{1}H} NMR *singlet* was observed at 55.1 ppm, rather than the A_2X pattern predicted on the basis of the square pyramidal geometry of Scheme 2. This singlet undergoes no change in multiplicity even on cooling to –90 °C. We confirmed that the square pyramidal

Scheme 2.

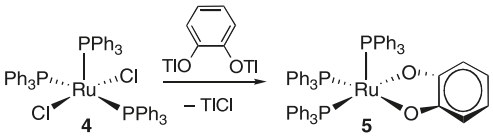

Scheme 3.

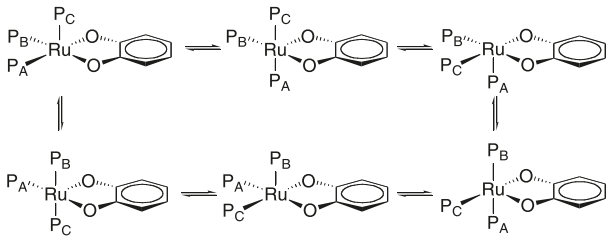

coordination geometry represents the energetic minimum by DFT optimization. The steric constraints in **5** may thus cause averaging of the ^{31}P environments in solution, via a series of equilibria such as those depicted in Scheme 3. Notably, no loss of PPh_3 in solution is evident by NMR analysis, despite this steric pressure, and in contrast to the behaviour of the corresponding dichloride complex **4** (6). This point is examined in more detail below.

Blocky blue crystals of **5** suitable for X-ray analysis were obtained by slow evaporation of a benzene solution. An ORTEP diagram is shown in Fig. 2 with crystal data in Table 1. Only one five-coordinate Ru-catecholate complex, Ru(o-cat)$_2$(≡N) **6** (7), has previously been structurally characterized. In contrast with the slightly distorted square pyramidal geometry of **6**, in which the nitrido ligand is only 0.6 Å above the basal plane, the structure of **5** exhibits significant deviations, though it remains closer to square pyramidal than trigonal bipyramidal at Ru. Two "basal" PPh_3 ligands lie trans to the catecholate oxygen donors (P(1)-Ru(1)-O(1) = 144.61(4)°; P(2)-Ru(1)-O(2) = 158.53(4)°), with the third phosphine approximately apical (P(3)-Ru(1)-P(1) = 97.766(17)°; P(3)-Ru(1)-P(2) = 99.561(17)°; P(3)-Ru(1)-O(1) = 116.13(4)°; P(3)-Ru(1)-O(2) = 98.45(4)°), trans to the vacant site. The extent of distortion is also evident from the 0.05 Å difference in length between the two Ru–P bonds in the basal plane (Ru(1)–P(1) 2.2954(5) Å; Ru(1)–P(2) 2.3496(5) Å). The apical Ru–P bond (Ru(1)–P(3) 2.2527(5) Å) is shorter by 0.04–0.09 Å. This is *not* due to population of the Ru-P(3) σ*-orbital (LUFO+1 of $[Ru(PPh_3)_3]^{2+}$): while there is indeed a 19% population of this orbital, the basal Ru–P bonds are likewise populated and to a greater extent (22% for LUFO; 11% for LUFO+2). Instead, the decreased bond length is due to the apical position of the phosphine ligand involved, and the consequent absence of a trans ligand that would give rise to a competing donor–acceptor interaction. A similar effect was found for the apical Ru–P bond in the dichloride analogue **4** (6).

The distorted geometry of **5** is unsurprising, given the rigidity and small bite angle of the catecholate ligand and the unfavourable steric interaction between the three cis-PPh_3 ligands. In comparison, the crystal structure of **4**, containing a meridional arrangement of these ligands, shows little distortion in the bond angles about ruthenium (6). Similarly,

Fig. 2. ORTEP diagram for Ru(*o*-cat)(PPh_3)$_3$ **5**·C_6H_6. Thermal ellipsoids at 50% probability; hydrogen atoms omitted for clarity.

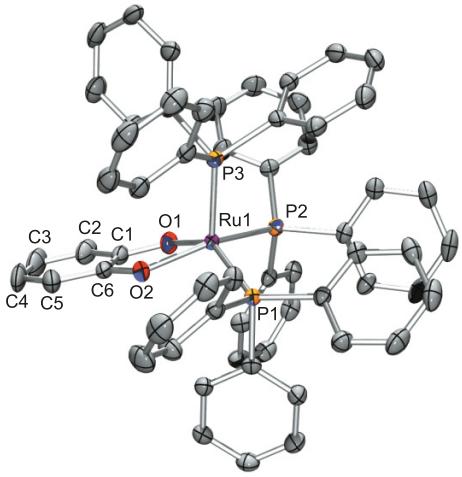

Table 1. Crystal data and structure refinement for **5**·C_6H_6

Formula	$C_{66}H_{55}O_2P_3Ru$
Formula mass	1074.08
Size (mm)	0.6 × 0.44 × 0.42
Colour, crystal morphology	Blue, block
Temperature (K)	173(2) K
Wavelength (Å)	0.710 73
Crystal system, space group	Monoclinic, $P2_1/c$
a (Å)	13.3727(13)
b (Å)	17.1572(18)
c (Å)	23.022(2)
α (°)	90
β (°)	94.653(3)
γ (°)	90
Volume (Å^3)	5264.7(9)
Z, calcd. density (mg/m^3)	4, 1.355
Absorption coefficient (mm^{-1})	0.435
F(000)	2224
Data collection range	1.48° ≤ θ ≤ 27.07°
Index ranges	–17 ≤ h ≤ 12, –17 ≤ k ≤ 21, –22 ≤ l ≤ 28
Reflections collected	21 831
Independent reflections	10 952 [R(int) = 0.0224]
Observed reflections	9287 [$I > 2\sigma(I)$]
Absorption correction	Multi-scan
Max. and min. transmission	0.8383 and 0.7802
Refinement method	Full
Data, restraints, parameters	10 952, 0, 649
Goodness of fit	1.032
Final R indices [$I > 2\sigma(I)$]	R_1 = 0.0286, wR_2 = 0.0716
R indices (all data)	R_1 = 0.0375, wR_2 = 0.075
Largest diff. peak and hole (e Å^{-3})	0.558 and –0.279

six-coordinate Ru(II)-catecholate complexes containing smaller neutral ligands such as PMe_3 (8) or pyridine (9) form reasonably regular octahedral complexes. The C–O bond

Fig. 3. Experimental and calculated electronic spectra for **5** (solid black and red lines, respectively) and calculated spectrum for **7** (dashed red line).

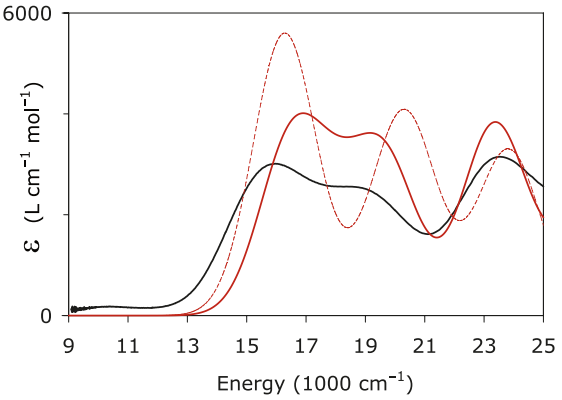

lengths within **5** (1.350(2) and 1.345(2) Å for C(1)–O(1) and C(6)–O(2), respectively) are within the range of 1.34–1.47 Å usual for Ru-catecholate complexes; benzoquinone complexes exhibit shorter C–O bond lengths (1.27–1.31 Å (10)). The magnitude and uniformity of C–C bond lengths within the $O_2C_6H_4^{2-}$ ligand (1.372(4)–1.407(4) Å) likewise support formulation of **5** as a Ru-catecholate complex, as does the presence of an IR band for $\nu_{C\text{-}O}$ at 1270 cm^{-1}, which is not observed for starting **4**, but is present in the IR spectra of the catecholate salts.

The electronic structure of **5** was analyzed experimentally by UV–vis spectroscopy and theoretically by use of TD-DFT calculations (11–13) to establish the key metal-ligand bonding contributions. Our interest was stimulated further by the unusual blue color of **5**, rare in Ru(II) complexes (for examples see refs. 14–21), which could provide added insight into its properties. A fragment molecular orbital (FMO) analysis enabled the quantification of charge donation. Orbital interactions were considered in terms of dative bonds between the lowest unoccupied fragment orbitals (LUFOs) of the metal fragment $[Ru(PPh_3)_3]^{2+}$ and the highest occupied fragment orbitals (HOFOs) of the $O_2C_6H_4^{2-}$ ligand.

The calculated electronic spectrum is in very good agreement with the experimental spectrum (Fig. 3). The latter, measured in THF, is comprised of three absorption maxima of near-identical intensity (16 000, 18 400, and 23 500 cm^{-1}), whereas TD-DFT predicts three principal bands (16 500, 19 700, and 23 200 cm^{-1}), of which the latter two overlap with two weaker bands at 18 000 and 23 600 cm^{-1}. The band energies thus correspond within ca. 500 cm^{-1} vs. the more typical agreement of 2 000 cm^{-1} (11–13, 22); a minor difference in intensity is also evident. The level of theory was therefore deemed appropriate for the analysis of the electronic transitions. Electron excitations contributing to each band are summarized in Table 2.

The FMO analysis indicates that the formation of **5** involves a significant (>2%) change in the electronic population for only three orbitals on the Ru fragment. We therefore confine our discussion of the metal-based orbital interactions to these three acceptor orbitals. Contributions from Ru are cited as the composite of s, p, and d contributions; those from PPh_3 are largely p in character (for individual constitu-

Table 2. Electron excitations contributing to bands in the visible region for **5**.

		(TD-DFT (B3LYP/DZVP))	
Exptl. energy[a]	Calcd. energy[a]	f[b]	Assignment[c]
16.0	16.5	0.0370	H→L (44%), H-2→L (29%), H-1→L (10%)
18.4	18.0	0.0190	H-1→L (57%), H→L (17%)
	19.7	0.0338	H-2→L (45%), H-3→L (24%)
			H→L (15%)
23.5	23.2	0.0272	H-3→L (31%), H-4→L (20%)
			H→L+1 (15%)
	23.6	0.0166	H→L+1 (47%)

[a]Band locations in 10^3 cm^{-1}.
[b]Oscillator strength.
[c]H = HOMO; L = LUMO. Only major (> 10%) parent one-electron excitations shown; percentage contributions to wavefunctions of excited states in parentheses.

Fig. 4. Lowest unoccupied fragment orbitals (LUFOs) of $[Ru(PPh_3)_3]^{2+}$ and their compositions (excluding phenyl ontributions). Isosurface contour value for orbital images 0.03 au.

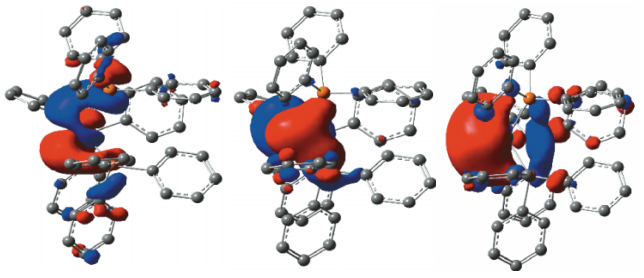

Table 3. Molecular orbital energies (E) and atomic contributions for **4** and **5**.

Orbital	$-E$ (eV)	Ru (%)	PPh_3 (%)	X-ligand (%)
4, LUMO	2.03	47.3	47.6	5.1
4, HOMO	5.10	55.6	5.9	38.5
5, LUMO +1	1.07	7.0	91.5	1.5
5, LUMO	1.81	38.5	49.1	12.4
5, HOMO	4.62	12.8	8.5	78.7
5, HOMO –1	5.26	34.3	7.9	57.8
5, HOMO –2	5.43	46.5	11.8	41.7
5, HOMO –3	5.80	53.3	16.9	29.8
5, HOMO –4	6.13	59.3	12.9	27.8

Note: Atomic contributions evaluated by Mulliken population analysis.

ents see Fig. 4). The LUFO is 62% Ru and 38% PPh_3 (of which 21% is contributed from the P atoms) in character; cf. relative contributions of 58% Ru + 42% PPh_3 for LUFO+1, and 59% Ru + 40% PPh_3 for LUFO+2. The population of each of these orbitals increases from its null value in the non-interacting fragment to 22%, 19%, and 11%, respectively, in **5**. LUFO and LUFO+2 participate in forming the two σ bonds with the ligand, while LUFO+1 forms a π bond (19% × 2 = 0.38 e^-). For the catecholate FMOs, turning on the bonding interaction with Ru results in a significant change in population for six occupied and one unoccupied orbital. These are the HOFO (–21%, i.e., 21% depopulation), HOFO–1 (–14%), HOFO–2 (–7%), HOFO–3 (–3%), HOFO–6 (–5%), HOFO–7 (–4%), and LUFO (+5% population). Thus, in addition to strong ligand-to-metal charge donation (0.94 e^-), formation of the complex involves significant polarization of the electron density on the catecholate ligand through 5% population of the LUFO. This charge distribution description is consistent with the Mulliken population analysis (23–26) and the NPA-derived charges assessed for the catecholate ligand in the complex (–1.06 and –1.20 au, respectively; NPA = natural population analysis).

The molecular orbitals that contribute to the visible spectrum of **5** are summarized in Table 3; visual depictions of all of these are given in the supporting information.[4] The LUMO is a σ* orbital for the apical Ru-PPh_3 bond (Fig. 5), while LUMO+1 consists principally of the aromatic π* orbitals of PPh_3 with a 7% contribution from the Ru 4d orbitals. The low energy of the LUMO of **5** derives from the contribution of a single (apical) phosphine ligand to this σ* orbital (p_z(P)–d_{z2}(Ru)); the other σ* orbital involves both basal PPh_3 ligands. The HOMO is a π bonding orbital between the catecholate and Ru. HOMO-1, HOMO-2, and HOMO-3 are also dominated by Ru-catecholate contributions: these are a largely non-bonding π orbital, a largely σ nonbonding orbital, and a σ–π hybrid, respectively. Finally, HOMO-4 is nonbonding, being composed of a Ru d orbital and the catecholate π orbital.

For four of the five visible bands calculated for **5**, the LUMO (σ* orbital of the apical Ru-PPh_3 bond) participates

[4]Supplementary data contains molecular orbitals implicated in the visible spectrum of **5**; tables of crystal data collection and refinement parameters, atomic coordinates, bond lengths, and angles, anisotropic displacement parameters and hydrogen coordinates, and NMR spectra for **5**. Supplementary data for this article are available on the journal Web site (canjchem.nrc.ca) or may be purchased from the Depository of Unpublished Data, Document Delivery, CISTI, National Research Council Canada, Ottawa, ON K1A 0R6, Canada. DUD 3854. For more information on obtaining material refer to cisti-icist.nrc-cnrc.gc.ca/cms/unpub_e.shtml. CCDC 689209 contains the crystallographic data for this manuscript. These data can be obtained, free of charge, via www.ccdc.cam.ac.uk/conts/retrieving.html (Or from the Cambridge Crystallographic Data Centre, 12 Union Road, Cambridge CB2 1EZ, UK; fax +44 1223 336033; or deposit@ccdc.cam.ac.uk).

Fig. 5. Frontier orbitals for (*a*) **4** and (*b*) **5**. Isosurface contour value for orbital images = 0.03 au.

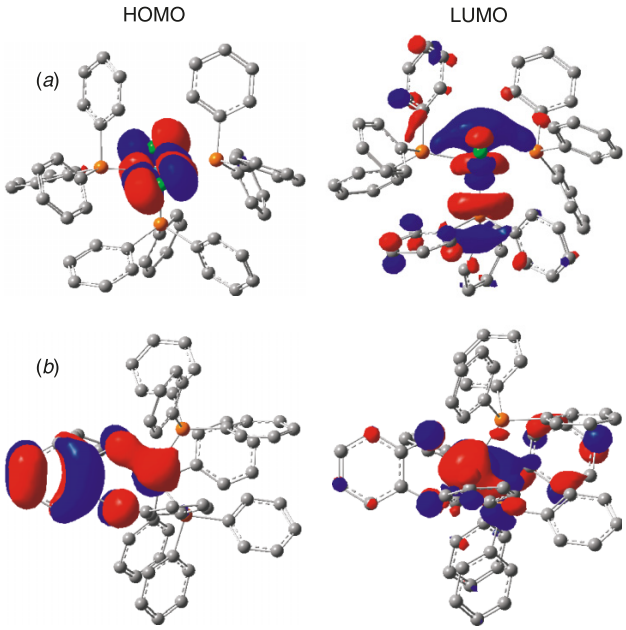

in the electronic excitations. However, the LUMO+1, composed of the π* orbitals of the aromatic rings of the PPh_3 ligands (Table 3), is also implicated in the absorption bands at 23 200 and 23 600 cm^{-1}. To determine whether this orbital plays a significant role in the electronic spectrum, we calculated the electronic spectrum of Ru(*o*-cat)$(PMe_3)_3$ (**7**), which contains no π*(Ph) orbitals. The calculated spectra for **5** and **7** are very similar, as shown in Fig. 3 (**7**: three absorption maxima at 16 300, 20 400, and 23 800 cm^{-1}; cf. the values for **5** noted above). We conclude that the LUMO is more critical to the spectroscopic features in the visible region than is LUMO+1. The intense blue colour of **5** (ε 3000 L $mol^{-1}cm^{-1}$) is thus due to charge transfer from the Ru-catecholate π bond (localized mostly on catecholate) to the low-lying σ* orbital on the apical Ru-PPh_3 bond.

Replacing the two chloride ligands in **4** by catecholate reduces the magnitude of the HOMO–LUMO gap, as evidenced by the change in colour from brown to blue. Consistent with this, the calculated values drop from –3.06 eV for **4** to –2.81 eV for **5**. The coordination number also affects the energy of the relevant electronic transitions, as noted above; Ru(*o*-cat)$(PMe_3)_4$ (8) and Ru(*o*-cat)$(py)_4$ (9), for example, are yellow in colour. While crystallographic analysis has demonstrated that a phenyl ring blocks the sixth coordination site in the solid state for **4**, the Ru–H distance (2.82 Å, corresponding to a bond order of 0.03) precludes the presence of an agostic C–H bond (27). We therefore exclude octahedral coordination as a potential explanation for the higher-energy visible transition for **4**. The smaller HOMO–LUMO gap in **5** is thus due principally to the higher energy of the HOMO, the Ru-P_{apical} σ* LUMO interaction being less affected, as shown in Fig. 5 and Table 3.

While the smaller HOMO–LUMO gap present in **5** might be expected to heighten reactivity, the resistance of this complex to loss of PPh_3 is in striking contrast to the behaviour of **4** (phosphine dissociation being the stepping-stone to the rich coordination chemistry of this classic ruthenium precursor (28)). The low lability of the PPh_3 ligand in **5**, evident by NMR analysis, is further supported by the unreactivity of the complex toward terminal alkynes, a facile, high-yield route to cumulenylidene products for **4** (29). The difference in behaviour lies in the stronger donation and back-donation involving the basal PPh_3 ligands in **5**, which result in a larger binding energy for Ru-$P_{(basal)}$ (–16.0 kcal mol^{-1} in **5** and –10.6 kcal mol^{-1} in **4**) (1 cal = 4.184 J). The weaker donation from the catechol ligand, relative to chloride, is anticipated on the basis of the higher electronegativity of oxygen vs. chlorine, reinforced by the capacity of the catecholate phenyl ring to delocalize negative charge. Consistent with this view, the NPA-derived charge for the catecholate ligand is –1.20 au, while for the chloride ligands the corresponding sum charge is –1.11 au.

Summary

The foregoing demonstrates that replacing chloride by catecholate in the simple model system $RuCl_2(PPh_3)_3$ raises the energy of the X-based HOMO. By analogy, replacing chloride by catecholate in Ru metathesis catalysts is expected to raise the energy of the corresponding Ru-X occupied molecular orbital(s). While the nature and energy of the frontier molecular orbitals in Ru metathesis catalysts has been surprisingly little examined (30), it is clear that the higher energy of the Ru-OAr HOMO will facilitate interaction with any LUMOs of appropriate symmetry present (which may include those for the alkylidene and bound olefin as well as the neutral donor that serves as a proxy for incoming olefin). These amplified interactions enhance the potential for modulating reactivity and selectivity by tuning the electronic properties of the anionic donors. Important steps in the catalytic cycle for olefin metathesis that may be affected range from dissociation of the neutral donor (in **3**, the pyridine ligand), to olefin binding and activation, and potentially, the key 2+2 cycloaddition step. Of additional interest is the extent to which the energy of the Ru-X (catecholate) HOMO is affected by the constrained bond geometry of the catecholate ligand. Future work will explore the specifics of these interactions, and their impact on the energy profile for metathesis in the $RuX_2(IMes)(py)(=CH_2)$ family of catalysts (X = Cl, *o*-cat, OC_6F_5).

Experimental

General procedures

Synthesis of **5** was carried out at room temperature (RT) (23 °C) under N_2 using standard drybox techniques. Dry, oxygen-free solvents, obtained using a Glass Contour solvent purification system, were stored over Linde 4 Å molecular sieves. Thallium catecholate (3*d*) and $RuCl_2(PPh_3)_3$ (31) were prepared by the methods reported.

^1H NMR (500 MHz), ^{13}C (125 MHz), and ^{31}P (121 MHz) spectra were recorded on a Bruker Avance-500 spectrometer. Chemical shifts are reported relative to TMS (^1H, ^{13}C) or 85% H_3PO_4 (^{31}P) at 0 ppm. X-ray data were collected on a Bruker SMART 1000 CCD diffractometer. IR spectra were measured on a Bomem MB100 IR spectrometer. Inert-atmosphere MALDI-MS analyses were carried out using a

Bruker OmniFlex MALDI-TOF mass spectrometer equipped with an N_2 laser (337 nm), interfaced to an MBraun glovebox (5). Data were collected in positive reflectron mode, with the accelerating voltage held at 20 kV. Matrix (pyrene) and analyte solutions were prepared in CH_2Cl_2 at concentrations of 20 and 1 mg/mL, respectively. Samples were mixed in a matrix/analyte ratio of 20:1. UV–vis spectra were measured on a Varian Cary-50 spectrophotometer at a scan rate of 600 nm/min. Samples were prepared under N_2 by filling a Hellma screw-top optical glass cell with 2 mL of a 0.24 mmol/L solution of **5** in THF and sealing prior to analysis. Microanalyses were carried out by Guelph Chemical Laboratories Ltd., Guelph, Ontario, Canada.

Note: The toxicity of thallium (particularly in the +1 oxidation state) is well-established (32). Care must be taken to prevent introduction into the body by inhalation, ingestion, or through the skin. All thallium reagents and wastes, including contaminated solvents, were handled using double-glove and secondary containment procedures, with separate disposal of all wastes in accordance with government regulations.

Synthesis of Ru(κ^2-*O,O′*-$O_2C_6H_4$)(PPh_3)$_3$ 5

Solid thallium catecholate (296 mg, 0.573 mmol) was added to a stirred solution of **4** (500 mg, 0.521 mmol) in 10 mL THF at RT. A colour change from brown to blue took place over 1 h, and the solution became cloudy. The suspension was filtered through Celite to remove TlCl, and the filtrate stripped to dryness. Precipitation from THF–hexanes and washing with hexanes (3 × 5 mL) afforded deep blue **5**. Yield 486 mg (94%). ^{1}H NMR (C_6D_6, 500 MHz) δ: 7.39 (m, 2H, catechol CO-C*H*), 7.30 (m, 18H, *o*-C*H* of PPh_3), 7.02 (m, 2H, catechol C*H*), 6.90 (m, 9H, *p*-C*H* of PPh_3), 6.74 (m, 18H, *m*-C*H* of PPh_3). ^{13}C{^{1}H} NMR (C_6D_6, 125 MHz) δ: 163.3 (s, catechol *C*-O), 137.4–137.1 (m, *i-C* of PPh_3), 135.3–135.2 (m, *o-C*H of PPh_3), 128.9 (s, *p-C*H of PPh_3), 127.5–127.4 (m, *m-C*H of PPh_3), 117.6 (s, catechol *C*H), 117.5 (s, catechol *C*H). ^{31}P{^{1}H} NMR (C_6D_6, 121 MHz) δ: 55.1 ppm (s); multiplicity unchanged down to –90 °C. IR (Nujol, cm^{-1}): $\nu_{C\text{-}O}$ 1270. Anal. calcd. for $C_{60}H_{49}O_2P_3Ru$: C 72.35, H 4.96%; found C 72.08, H 4.85%. MALDI-MS, *m/z* (pyrene matrix): calcd. for [M-PPh_3]$^{+\cdot}$: 734.1; found, 734.4.

Representative reaction of 5 and 3,3-dimethylbutyne

To a blue solution of **5** (14 mg, 0.014 mmol) in C_6D_6 (1 mL) was added 3,3-dimethylbutyne (10 μL, 0.084 mmol, 6 equiv). The reaction vessel was sealed and heated to 60 °C in an aluminum block for up to 72 h, after which NMR analysis showed only unreacted **5**.

Representative reaction of 5 with 1,1-diphenylprop-2-yn-1-ol

To a blue solution of **5** (25 mg, 0.025 mmol) in THF (2 mL) was added solid 1,1-diphenylprop-2-yn-1-ol (6 mg, 0.029 mmol, 1.2 equiv). No reaction was evident by NMR analysis at RT over a period of 24 h. Only the ^{31}P NMR signal for **5** was present after heating for 1 h in an oil bath set at 70 °C. Complex **5** remains a major species after heating for 17 h, but it is accompanied by multiple products, suggesting sample decomposition. Similar results were found on use of up to 5 equiv of the alkyne.

Structural determination

Blue, blocky crystals of **5** were grown by slow evaporation of a saturated benzene solution. Data were collected on a Bruker SMART 1000 CCD diffractometer with Mo Ka radiation using the ω-scan mode. A single crystal (0.6 mm × 0.44 mm × 0.42 mm) was mounted on a thin glass fiber using paraffin oil and cooled to the data collection temperature (173 K). Data were corrected using the SADABS program (Bruker). Structure solution in the space group $P2_1/c$ was performed with Patterson methods, completed with difference Fourier syntheses, and refined by full-matrix least-squares procedures based on F^2 using the SHELX-97 software package. All non-hydrogen atoms were refined anisotropically; hydrogen atoms were placed at geometrically calculated positions and allowed to ride on their parent atoms. Although the crystals were weakly diffracting, a satisfactory structural solution was obtained.

Computational details

DFT calculations were carried out using the Gaussian 03 package (33). The X-ray structures of **4** (27*b*) and **5** were used for these calculations, after adjusting all C–H distances to 1.08 Å, as only aromatic C–H bonds are present in the structure. All other interatomic distances were left unperturbed. That the square pyramidal structure represents a true energy minimum for **5** was confirmed by geometry optimization. DFT calculations utilized the B3LYP (34) exchange-correlation functional with the DZVP basis set (35) for all atoms. Tight SCF convergence criteria (10^{-8} au) were used for all calculations. The converged wave functions were tested to confirm that they correspond to the ground-state surface. Bond orders and the compositions and populations of molecular orbitals were calculated using the AOMix program (36). The energies and intensities of the lowest 30 singlet-singlet transitions were calculated by TD-DFT. Absorption profiles were calculated from TD-DFT bands by the method reported (22), assuming for all electronic transitions a bandwidth at half-height of 2500 cm^{-1} (a typical value for complexes of the type described). Pseudo-Voigt functions with 50% weights for contributing Gaussian and Lorentzian functions were used to simulate the absorption bands.

Acknowledgements

This work was supported by Natural Sciences and Engineering Research Council of Canada (NSERC) of Canada, the Canada Foundation for Innovation, and the Ontario Innovation Trust. NSERC and Coordenação de Aperfeiçoamento de Pessoal de Nível Superior (CAPES) and Conselho Nacional de Desenvolvimento Científico e Tecnológico (CNPq) of Brazil are acknowledged for fellowships to SM and JDS.

References

1. Please see these leading reviews: (*a*) R.H. Grubbs. Handbook of metathesis. Wiley-VCH, Weinheim, Germany. 2003; (*b*) K.C. Nicolaou, P.G. Bulger, and D. Sarlah. Angew. Chem. Int. Ed. **44**, 4490 (2005); (*c*) R.R. Schrock. Angew. Chem. Int.

Ed. **45**, 3748 (2006); (*d*) R.H. Grubbs. Angew. Chem. Int. Ed. **45**, 3760 (2006).
2. For exceptions, see: (*a*) R. Gawin, A. Makal, K. Wozniak, M. Mauduit, and K. Grela. Angew. Chem. Int. Ed. **46**, 7206 (2007); (*b*) N. Ledoux, R. Drozdzak, B. Allaert, A. Linden, P. Van Der Voort, and F. Verpoort. Dalton Trans. 5201 (2007); (*c*) J.O. Krause, O. Nuyken, K. Wurst, and M.R. Buchmeiser. Chem. Eur. J. **10**, 777 (2004); (*d*) M.S. Sanford, J.A. Love, and R.H. Grubbs. J. Am. Chem. Soc. **123**, 6543 (2001).
3. (*a*) J.C. Conrad, D. Amoroso, P. Czechura, G.P.A. Yap, and D.E. Fogg. Organometallics, **22**, 3634 (2003); (*b*) J.C. Conrad, H.H. Parnas, J.L. Snelgrove, and D.E. Fogg. J. Am. Chem. Soc. **127**, 11882 (2005); (*c*) J.C. Conrad, M.D. Eelman, J.A. Duarte Silva, S. Monfette, H.H. Parnas, J.L. Snelgrove, and D.E. Fogg. J. Am. Chem. Soc. **129**, 1024 (2007); (*d*) S. Monfette and D.E. Fogg. Organometallics, **25**, 1940 (2006).
4. (*a*) J.L. Snelgrove, J.C. Conrad, M.M. Moriarty, G.P.A. Yap, and D.E. Fogg. Organometallics, **24**, 103 (2005); (*b*) J.L. Snelgrove, J.C. Conrad, G.P.A. Yap, and D.E. Fogg. Inorg. Chim. Acta, **345**, 268 (2003), and refs. cited therein; (*c*) D.J. Cole-Hamilton, R.J. Young, and G. Wilkinson. J. Chem. Soc. Dalton Trans. 1995 (1976).
5. M.D. Eelman, J.M. Blacquiere, M.M. Moriarty, and D.E. Fogg. Angew. Chem. Int. Ed. **47**, 303 (2008).
6. P.R. Hoffman and K.G. Caulton. J. Am. Chem. Soc. **97**, 4221 (1975).
7. G.-S. Fang, J.-S. Huang, N. Zhu, and C.-M. Che. Eur. J. Inorg. Chem. 1341 (2004).
8. M. Hirano, H. Sato, N. Kurata, N. Komine, and S. Komiya. Organometallics, **26**, 2005 (2007).
9. H. Masui, A.B.P. Lever, and P.R. Auburn. Inorg. Chem. **30**, 2402 (1991).
10. O. Carugo, C.B. Castellani, K. Djinovic, and M. Rizzi. J. Chem. Soc. Dalton Trans. 837 (1992).
11. M.E. Casida. Recent Adv. Comput. Chem. **1**, 155 (1995).
12, M.E. Casida. Theor. Comput. Chem. **4**, 391 (1996).
13. R.E. Stratmann, G.E. Scuseria, and M.J. Frisch. J. Chem. Phys. **109**, 8218 (1998).
14. E.J. Derrah, D.A. Pantazis, R. McDonald, and L. Rosenberg. Organometallics, **26**, 1473 (2007).
15. P. Banerjee, S. Das, P.E. Fanwick, and S. Goswami. J. Organomet. Chem. **691**, 2915 (2006).
16. S. Jasimuddin, P. Byabartta, C. Sinha, G. Mostafa, and T.-H. Lu. Inorg. Chim. Acta **357**, 2015 (2004).
17. C. Das, A. Saha, C.-H. Hung, G.-H. Lee, S.-M. Peng, and S. Goswami. Inorg. Chem. **42**, 198 (2003).
18. P. Byabartta, S. Jasimuddin, B.K. Ghosh, C. Sinha, A.M.Z. Slawin, and J.D. Woollins. New J. Chem. **26**, 1415 (2002).
19. R.-A. Fallahpour and M. Neuburger. Helv. Chim. Acta, **84**, 715 (2001).
20. K. Mashima, H. Kaneyoshi, S.-i. Kaneko, A. Mikami, K. Tani, and A. Nakamura. Organometallics, **16**, 1016 (1997).
21. H. Tom Dieck, W. Kollvitz, and I. Kleinwaechter. Inorg. Chem. **23**, 2685 (1984).
22. S.I. Gorelsky and A.B.P. Lever. J. Organomet. Chem. **635**, 187 (2001).
23. R.S. Mulliken. J. Chem. Phys. **23**, 2343 (1955).
24. R.S. Mulliken. J. Chem. Phys. **23**, 2338 (1955).
25. R.S. Mulliken. J. Chem. Phys. **23**, 1841 (1955).
26. R.S. Mulliken. J. Chem. Phys. **23**, 1833 (1955).
27. (*a*) S.J. LaPlaca and J.A. Ibers. Inorg. Chem. **4**, 778 (1965); (*b*) CCDC file number 214959.
28. E.A. Seddon and K.R. Seddon. The chemistry of ruthenium. Elsevier, Amsterdam. 1984.
29. Please see these representative reports: (*a*) D. Touchard, S. Guesmi, M. Bouchaib, P. Haquette, A. Daridor, and P.H. Dixneuf. Organometallics, **15**, 2579 (1996); (*b*) Y. Wakatsuki, N. Koga, H. Yamazaki, and K. Morokuma. J. Am. Chem. Soc. **116**, 8105 (1994); (*c*) A. Keller, B. Jasionka, T. Glowiak, A. Ershov, and R. Matusiak. Inorg. Chim. Acta, **344**, 49 (2003); (*d*) K.J. Harlow, A.F. Hill, and J.D.E.T. Wilton-Ely. J. Chem. Soc. Dalton Trans. 285 (1999).
30. C.H. Suresh and N. Koga. Organometallics, **23**, 76 (2004).
31. P.S. Hallman, T.A. Stephenson, and G. Wilkinson. Inorg. Synth. **12**, 237 (1970).
32 S. Galvan-Arzate and A. Santamaria. Toxicol. Lett. **99**, 1 (1998).
33. M.J. Frisch, G.W. Trucks, H.B. Schlegel, G.E. Scuseria, M.A. Robb, J.R. Cheeseman, J.A. Montgomery, Jr., T. Vreven, K.N. Kudin, J.C. Burant, J.M. Millam, S.S. Iyengar, J. Tomasi, V. Barone, B. Mennucci, M. Cossi, G. Scalmani, N. Rega, G.A. Petersson, H. Nakatsuji, M. Hada, M. Ehara, K. Toyota, R. Fukuda, J. Hasegawa, M. Ishida, T. Nakajima, Y. Honda, O. Kitao, H. Nakai, M. Klene, X. Li, J. E. Knox, H.P. Hratchian, J.B. Cross, C. Adamo, J. Jaramillo, R. Gomperts, R.E. Stratmann, O. Yazyev, A.J. Austin, R. Cammi, C. Pomelli, J.W. Ochterski, P.Y. Ayala, K. Morokuma, G.A. Voth, P. Salvador, J.J. Dannenberg, V.G. Zakrzewski, S. Dapprich, A.D. Daniels, M.C. Strain, O. Farkas, D.K. Malick, A.D. Rabuck, K. Raghavachari, J.B. Foresman, J.V. Ortiz, Q. Cui, A.G. Baboul, S. Clifford, J. Cioslowski, B.B. Stefanov, G. Liu, A. Liashenko, P. Piskorz, L. Komaromi, R.L. Martin, D.J. Fox, T. Keith, M.A. Al-Laham, C.Y. Peng, A. Nanayakkara, M. Challacombe, P.M. W. Gill, B. Johnson, W. Chen, M.W. Wong, C. Gonzalez, J.A. Pople. Gaussian 03. Revision B.04 [computer program]. Gaussian, Inc., Pittsburgh, Penn., USA. 2003.
34. (*a*) A.D. Becke. J. Chem. Phys. **98**, 5648 (1993); (*b*) B. Miehlich, A. Savin, H. Stoll, and H. Preuss. Chem. Phys. Lett. **157**, 200 (1989); (*c*) C. Lee, W. Yang, and G. Parr. Phys. Rev. B, **37**, 785 (1988).
35. N. Godbout, D.R. Salahub, J. Andzelm, and E. Wimmer. Can. J. Chem. **70**, 560 (1992).
36. S.I. Gorelsky. AOMix: Program for molecular orbital analysis. Version 6.35. University of Ottawa, Ottawa, Ont., Canada. 2007.